# Shaping of Axisymmetric Bodies for Minimum Drag in Incompressible Flow

Jerome S. Parsons* and Raymond E. Goodson†
*Purdue University, Lafayette, Ind.*
and
Fabio R. Goldschmied‡
*Westinghouse Electric Corporation, Pittsburgh, Pa.*

**A method is presented for the automatic synthesis of minimum drag hull shapes for axisymmetric vehicles of specified enclosed volume and constant speed submerged in incompressible, nonseparating, noncavitating flow at zero incidence. The computer-oriented optimization procedure does not consider propulsion or maneuvering; drag reduction is accomplished solely through manipulation of the vehicle hull shape. The selected optimization formulation is a nongradient algorithm in a finite, constrained parameter space. This study considers an eight-parameter class of rounded-nose tail-boom bodies constrained to be well behaved as determined by previous hydrodynamic experience. The drag model, for nonseparating flows at zero incidence, is based on classical hydrodynamics and consists of computer programs from work available in the literature; the model is representative of state-of-the-art drag prediction methods. By exploiting laminar flow while avoiding turbulent separation, a body with a drag coefficient one-third below the best existing laminar design has been obtained. The evidence suggests that the method produces realistic hull shapes useful in engineering design. The optimization procedure is independent of any particular drag model so that the effects on minimum drag shapes due to alternate drag models can be studied.**

## Nomenclature

$a_i$ = component of parameter set $a_i$, $i = 1, \ldots, N$.
$a(L_i)$, $a(U_i)$ = for Complex Method, the temporary lower and upper parameter boundaries, respectively, used during the initial complex generation.
$C_D$ = drag coefficient defined as $\text{Drag}/(1/2\,\rho U_\infty{}^2 V^{2/3})$.
$C_f$ = skin friction coefficient defined as $\tau_w/(1/2\,\rho U_\infty{}^2)$.
$C_p$ = pressure coefficient defined as $(p - p_\infty)/(1/2\,\rho U_\infty{}^2)$.
$D$ = vehicle drag. Also maximum diameter of body $Y(X_m)$.
$f_r$ = fineness ratio defined as $L/D$ where $D$ is the maximum diameter.
$H$ = shape factor defined as $\delta^*/\theta$.
$K$ = number of vertices in $N$-dimensional complex figure of the Complex Method. Normally $K = 2N$.
$K_1$ = body curvature at $X_m$ defined as $d^2Y(X_m)/dX^2$.
$k_1$ = nondimensional curvature at $X_m$ defined as $(-2X_m{}^2/D)K_1 = (-2x_m{}^2 f_r)K_1 L$ where $D$ is the maximum diameter.
$k(1_m)$ = nondimensional curvature at $X_m$ in terms of mid-body coordinates. Defined in Eq. (4k).
$L$ = over-all body length.
$N$ = number of independent parameters. Equivalently, the dimensionality of the search space.
$NN$ = total number of body profile points used in drag computation.
$PF$ = performance function. For drag minimization $PF$ is the same as $C_D$.
$p$ = pressure impressed on the boundary layer.
$p_\infty$ = free-stream static pressure.
$R_i$ = profile radius at $X_i$ defined as $Y(X_i)$.
$R_n$ = radius of curvature at nose defined as $1/(d^2X/dY^2)$ at $X = 0$.
$R_S$ = running surface-length Reynolds number defined as $S\,u_e/\nu$.
$R_V$ = body volume Reynolds number defined as $V^{1/3}U_\infty/\nu$.
$R_\theta$ = momentum thickness Reynolds number defined as $\theta u_e/\nu$.
$r$ = radial coordinate of a point in the boundary layer defined as $r_o + y\cos\alpha$.
$r_i$ = nondimensional profile radius at $X_i$ defined as $2R_i/D = 2f_r\,R_i/L$.
$r_n$ = nondimensional radius of curvature at nose defined as $(4X_m/D^2)R_n = (4x_m f_r{}^2)R_n/L$.
$r_o$ = body radius. Same as $Y$.
$S$ = surface length. Same as $x$.
$S_i$ = profile slope at $X_i$ defined as $dY(X_i)/dX$.
$S_{\text{Total}}$ = total surface arc-length.
$s_i$ = nondimensional profile slope at $X_i$ defined as $[-(X_i - X_m)/(D/2 - R_i)]S_i = [-2f_r(x_i - x_m)/(l - r_i)]S_i$.
$s(i_a)$ = nondimensional profile slope at $X_i$ in terms of tail-boom aftbody coordinates. Defined in Eq. (4q).
$T$ = terminal profile radius defined as $Y(L)$.
$t$ = nondimensional terminal profile radius defined as $2T/D = 2f_r T/L$.
$u$ = tangential velocity component at a point $(x,y)$ in the boundary layer.
$u_e$ = local velocity at the edge of the boundary layer.
$U_\infty$ = freestream reference velocity, same as the specified constant design speed of vehicle.
$V$ = enclosed volume of vehicle.
$v$ = normal velocity component at a point $(x,y)$ in the boundary layer.
$X$ = axial coordinate along body centerline.
$X_i$ = axial location of inflection point.
$X_m$ = axial location of maximum diameter $D$.
$x$ = streamwise curvilinear coordinate for boundary layer. Same as $S$.
$x_i$ = nondimensional axial location of inflection point defined as $X_i/L$.
$x_m$ = nondimensional axial location of maximum diameter $D$ defined as $X_m/L$.
$Y$ = body radius. Same as $r_o$.
$y$ = normal curvilinear coordinate for boundary layer.

Received March 9, 1973; revision received April 12, 1974. The authors wish to acknowledge the support provided by the Westinghouse Electric Corporation and by the Office of Naval Research under Contract NOOO14-67-A-0226-0012 NR 041-423.

Index categories: Hydrodynamics; Marine Vessel Design (Including Loads); Marine Vessel Systems, Submerged.

*Graduate Research Assistant, Automatic Control Center, School of Mechanical Engineering; presently Member of Technical Staff, Bell Telephone Laboratories, Whippany, N.J.

†Professor and Director of Automatic Control Center, School of Mechanical Engineering; presently Chief Scientist, U.S. Department of Transportation, Washington, D.C.

‡Advisory Scientist, Research Laboratories Associate. Fellow AIAA.

$\alpha$ = angle between the surface tangent and the body centerline in a meridional plane. Search strategy expansion factor in Eq. (8).
$\delta$ = boundary-layer thickness defined as the $y$-distance for which $u/u_e = 0.995$.
$\delta^*$ = displacement thickness associated with momentum integral equation. Defined as $\int_0^\infty r/r_o(1 - u/u_e)dy$ for incompressible flow.
$\epsilon$ = eddy viscosity.
$\epsilon_2, \epsilon_3$ = relative tolerances used in search method
$\theta$ = momentum thickness associated with momentum integral equation and Young's formula for computing drag. Defined as $\int_0^\infty r/r_o\, u/u_e\,(1 - u/u_e)dy$ for incompressible flow.
$\mu$ = fluid dynamic viscosity.
$\nu$ = fluid kinematic viscosity.
$\rho$ = fluid density.
$\tau_w$ = wall shear stress.

## I. Introduction

A FUNDAMENTAL interest in the field of hydrodynamics is the reduction of submerged vehicle power requirements. This is accomplished, in general, by some combination of 1) vehicle hull shaping, 2) boundary-layer control; e.g., polymer injection[1] or slot suction, 3) efficient propulsion; e.g., a wake propeller or a suction slot with a stern jet,[2] and 4) efficient steering control consistent with hydrodynamic stability.

Items 1 and 2 attempt to reduce skin friction and pressure drag while item 3 attempts to extract energy lost to the fluid surrounding the vehicle. A complete systems design simultaneously takes into account hull shaping, boundary-layer control, propulsion, and steering control.[2] But the overwhelmingly complicated nature of the complete problem has prohibited the analytical systems design approach. Hydrodynamicists are forced to rely heavily on experimentally based methods to reduce submerged vehicle power requirements.

The present study formalizes a portion of the complete systems problem. Herein is developed a computer-oriented optimization procedure for synthesizing vehicle hull shapes producing minimum drag for a specified vehicle volume and a constant vehicle speed in incompressible, nonseparating, noncavitating flow at zero incidence. Since propulsion is not considered, drag rather than power is minimized. The results should guide the hydrodynamic designer in selecting a vehicle shape to be combined with the mechanisms for boundary layer control, propulsion, and steering. Typical applications are those deeply submerged vehicles, such as torpedoes and submarines, which carry a payload in an enclosed volume at a nominally fixed design speed.

The hydrodynamic problem considered here is made more tractable by restricting the analysis to the class of axisymmetric vehicle shapes without appendages immersed in nonseparating, axisymmetric flow (zero incidence). Nondimensionalizing the problem, the most convenient Reynolds number and drag coefficient definitions are, respectively, $R_V = U_\infty V^{1/3}/\nu$ and $C_D = D/(1/2\,\rho U_\infty{}^2 V^{2/3})$, where $U_\infty$ is the constant vehicle speed, $V$ is the vehicle's enclosed volume, $\nu$ is the fluid kinematic viscosity, $D$ is the vehicle drag, and $\rho$ is the fluid density.

The application of formal optimization methods to the drag minimization problem considered here has not appeared in the literature to date. One reason for this absence is the fact that no reliable drag model is available for arbitrary axisymmetric bodies in incompressible flow which may or may not be separating. More fundamentally, there is an incomplete understanding of the fluid flow physics in the boundary-layer transition region, in the turbulent boundary-layer development, in the turbulent boundary-layer separation region, and in the wake region following separation. All of these phenomena are of primary importance in drag prediction. In addition, there are other factors which complicate the prediction of drag in practice.[3] Examples are the effects of ambient turbulence, body surface waviness, and body vibration on the boundary-layer development. With the lack of reliable drag models, all published work to date directed toward the design of low-drag axisymmetric bodies in incompressible flow has been mainly experimental in nature. Two studies are noted here.

An experimental study of drag for a systematic series of axisymmetric bodies was reported by Gertler in 1950.[4] The series, known as "Series 58," is systematic in that five parameters characterizing the rounded-nose, pointed-tail shapes are perturbed one at a time about a selected "parent model." Twenty-four designs were tested by towing models through water at Reynolds numbers up to $R_V = 5 \times 10^6$ (7 ft$^3$ at 18 knots). Not considered in the study were bodies designed to reduce drag by exploiting laminar flow. It was believed that such flow could not be used effectively at the submarine Reynolds numbers ($R_V \simeq 3 \times 10^8$) to which the designs were to be extrapolated. The study concludes that the resistance of submerged streamlined bodies can be reduced by proper geometrical shaping, and presents a minimum resistance submarine hull shape for all turbulent flow.

A laminar flow shape for torpedo-type Reynolds numbers ($R_V \simeq 10^7$) was developed by North American Aviation, Inc., and was reported by Carmichael in 1966.[3] The purpose of the study was to determine if significant drag reduction was possible through shape manipulation alone. A formal shape-synthesizing procedure was not developed; rather, one body was designed based on NACA low drag airfoil shapes. The one model, dubbed the "Dolphin," was tested extensively by gravity-powered drop tests in the Pacific Ocean. A significant drag reduction was noted, the Dolphin having half the drag of a conventional torpedo at similar Reynolds numbers. The low drag was achieved primarily by the Dolphin's ability to maintain a long run of laminar boundary layer. This fact in itself is important since prior to the Dolphin testing it was generally accepted that no significant amount of laminar boundary layer flow could be maintained at such high Reynolds numbers. While the Dolphin is not a minimum drag shape, it certainly demonstrates the practicality of exploiting laminar boundary layers and body shaping in general to produce efficient low-drag designs, at least in the tested Reynolds number range.

This paper proposes and tests a drag minimization procedure for synthesizing low-drag hull shapes useful to the hydrodynamic designer. The problem divides naturally into three parts: the optimization formulation, the mathematical description of the vehicle hull shapes, and the drag model. The method is demonstrated by comparing a design with the best experimentally verified design available in the literature. It is emphasized that the method is independent of the drag model so that the effect of alternate drag models on minimum drag shapes can be studied.

## II. Parametric Formulation of the Optimization Problem

Once the reference Reynolds number $R_V$ is fixed for the zero incidence, nonseparating flow, the value of the drag coefficient $C_D$ depends only on the shape $Y(X)$ of the axisymmetric body; i.e.,

$$C_D = C_D[Y(X)] \tag{1}$$

where $X$ is the axial coordinate.

The fact that the drag computation is done by a com-

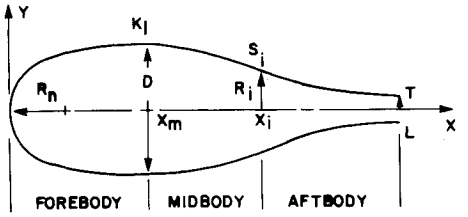


**Fig. 1 Example of the eight-parameter class of rounded-nose tailboom bodies with fixed boundary conditions used in the present study. Fixed boundary conditions: $Y(o) = 0$, $dY(o)/dx = \infty$; $dY(L)/dX = 0$; $d^2Y(L)/dX^2 = 0$.**

plex computer algorithm meant that an analytical optimization procedure such as Calculus of Variations would have to have strong positive benefits to justify its being used. After careful study it was decided that a parametric treatment provided the best balance of all the considerations.

As such, the general function $Y(X)$ is assumed to satisfy

$$Y(X) = Y\left(\sum_{i=1}^{N} a_i F_i(X), G(X)\right) \quad 0 \leq X \leq L \tag{2}$$

where $F_i(X)$ are a sequence of polynomials, $G(x)$ is chosen to satisfy boundary conditions, and $a_i$ are parameters to be determined. For a parameterically defined body the drag coefficient depends on the number $N$, the nature of the functions $F_i(X)$, and the multiplicative constants $a_i$, $i = 1, \ldots, N$. This may be expressed as

$$C_D = C_D[N, a_i, F_i(X);\ i = 1, \ldots, N] \tag{3}$$

Once $N$ and the $F_i(X)$, $i = 1, \ldots, N$, are fixed, it is possible to obtain minimum drag shapes for the restricted class defined by Eq. (2) by manipulating the set of constants $a_i$, $i = 1, \ldots, N$, in Eq. (3).

The formulation implied in Eqs. (2) and (3) requires solution by a parametric optimization method, whether using classical or other methods. By assuming the solution form to within a set of variable parameters, i.e., Eq. (2), the optimization results lose a degree of generality that the classical variational calculus solution retains. However, the parametric formulation has been adopted as the most feasible procedure for the drag minimization problem, particularly since the variational calculus approach appears to require an external iterative method to obtain an explicit solution. It is felt that the loss of generality of the parametric approach is not significant so long as the number of parameters $a_i$, $i = 1, \ldots, N$, is not unreasonably small.

## III. Mathematical Description of the Vehicle Hull Shape

In order to make a direct comparison between the present method and the best low-drag vehicle design available in the literature,[3] an eight-parameter class of rounded-nose, tailboom bodies has been developed. The procedures used to derive the analytic expression for $Y(X)$, i.e., Eq. (2), are essentially those reported by Granville in 1969.[5] The idea is to divide the body into sections, each described by a low degree polynomial. The complete body profile is continuous through the second derivative to avoid local regions of highly accelerated flow. The result of the lengthy analysis[6] is a class of rounded-nose, tailboom bodies completely described by a set of eight variable parameters.

An example of this class with its built-in boundary conditions is shown in Fig. 1. The forebody ($0 \leq X \leq X_m$) is described by a fourth-degree polynomial, the midbody ($X_m \leq X \leq X_i$) by a fifth-degree polynomial, and the tailboom aftbody ($X_i \leq X \leq L$) by a fifth-degree polynomial. The zero slope and curvature at $X = L$ allows a cylindrical tailboom extension to be added without loss of profile continuity through the second derivative. The body profile, open at $X = L$, is essentially a truncation of the complete body. For this body class, the short tailboom length seems to be an adequate approximation to the full tailboom for the purpose of computing the drag coefficient $C_D$ since the computed $C_D$ approaches a constant value near $X = L$ (see Sec. VI).

The nine parameters shown in Fig. 1 are reduced to the eight nondimensional, nonnegative parameters $r_n$, $f_r$, $x_m$, $k_l$, $x_i$, $r_i$, $s_i$, and $t$. The analytical expressions for this dimensionless eight-parameter body class are given below:

For $0 \leq X \leq X_m$ (forebody):

$$Y(X)/L = (1/2f_r)[r_n F_1(x) + k_1 F_2(x) + G(x)]^{1/2} \tag{4a}$$

where

$$x = X/X_m \tag{4b}$$

$$F_1(x) = -2x(x-1)^3 \tag{4c}$$

$$F_2(x) = -x^2(x-1)^2 \tag{4d}$$

$$G(x) = x^2(3x^2 - 8x + 6) \tag{4e}$$

For $X_m \leq X \leq X_i$ (midbody):

$$Y(X)/L = (1/2f_r)(r_i + (1 - r_i)[k_{1_m} F_1(x) + s_i F_2(x) + G(x)]) \tag{4f}$$

where

$$x = (X_i - X)/(X_i - X_m) \tag{4g}$$

$$F_1(x) = -1/2\ x^3(x-1)^2 \tag{4h}$$

$$F_2(x) = x - x^3(3x^2 - 8x + 6) \tag{4i}$$

$$G(x) = x^3(6x^2 - 15x + 10) \tag{4j}$$

$$k_{1_m} = [(x_i/x_m) - 1]^2 k_1/(1 - r_i) \tag{4k}$$

For $X_i \leq X \leq L$ (tailboom aftbody):

$$Y(X)/L = (r_i/2f_r)(1 + [(t/r_i) - 1]F_1(x) + s_{i_a} F_2(x)) \tag{4m}$$

where

$$x = (L - X)/(L - X_i) \tag{4n}$$

$$F_1(x) = 1 - x^3(6x^2 - 15x + 10) \tag{4o}$$

$$F_2(x) = -x^3(3x^2 - 7x + 4) \tag{4p}$$

$$s_{i_a} = (1 - r_i)(1 - x_i)s_i/(x_i - x_m)(r_i) \tag{4q}$$

A number of limiting type constraints, explicit in the dimensionless parameters, are placed on the eight-parameter class of rounded-nose, tailboom bodies. The constraints arise from physical limits as well as previous hydrodynamic experience. The role of the constraints is significant; they prevent the optimization strategy from finding low drag designs which are unrealistic or impractical in an engineering sense. These geometric constraints are summarized below:

1) $0 \leq r_n$
2) $0 \leq k_1$
3) $0 < x_m < x_i < 1$
4) $2.5 \leq f_r$, a somewhat arbitrary bound to help avoid separated flow on the body
5) $0 < t \leq r_i \leq 1$
6) $0 \leq s_i$
7) No inflection on forebody ($0 \leq X \leq X_m$); this requirement produces a nonlinear constraint boundary in $r_n - k_1$ space[5,6] (see Fig. 2).
8) No inflection on midbody ($X_m \leq X \leq X_i$) except at $X_i$; this requirement produces a nonlinear constraint boundary is $s_i - k_{1_m}$ space[6] (see Fig. 2).
9) No inflection on tailboom aftbody ($X_i \leq X \leq L$) except at $X_i$ and $L$; this requirement produces linear

constraint boundaries in $s(i_a) - (t/r_i)$ space[6] (see Fig. 2).

The inflection constraints (7–9) due to Granville,[5] are introduced primarily to maintain a smooth vehicle shape with a well-behaved streamwise pressure distribution.

An advantage of Granville's procedure of dividing the body into sections is now apparent; the two-dimensional constraints give geometric insight into the problem. The constrained body class is well behaved in that the body profiles are hydrodynamically smooth, i.e., continuous through the second derivative and without unwanted inflections. Other constraints are introduced by the numerical drag model discussed in Sec. IV.

## IV. Numerical Drag Model

The complicated physics involved in drag prediction can be divided into five parts: mainstream inviscid flow, laminar boundary layer flow, boundary layer transition, turbulent boundary layer flow, and turbulent boundary-layer separation. Methods for predicting mainstream inviscid flow and laminar boundary layers are well established. But there is less confidence in methods for predicting transition, turbulent boundary layers, and separation due to an incomplete understanding of the fundamental nature of the physics involved. Even so, reasonably good methods relying on some empirical correlations have appeared in the literature. We have used the method due to Smith, Cebeci, and their co-workers[7–11]; however, early in the project it was decided to develop the optimization strategy independent of any particular drag model so that future improvements in drag prediction methods could be incorporated into the minimization program if desired.

Following Cebeci,[7] the flow field and basic notation are shown in Fig. 3. The mainstream flow outside the boundary layer is accurately modeled by inviscid potential flow theory. The boundary layer is laminar from the leading edge to the transition point A and is assumed fully turbulent from point A to the trailing edge. Turbulent separation is not allowed; this requirement is a constraint on the optimization problem since the drag model is not valid for separated boundary layer flow. Turbulent boundary-layer separation is assumed to occur when the computed skin friction becomes negative causing the iterative solution to diverge. In addition, to help avoid separating flow, we have constrained the velocity ratio $u_e(x)/U_\infty$ not to exceed 1.2 in value for $0 \le X \le L$.

The mainstream inviscid velocity distribution along the body surface is computed using the Douglas-Neumann method[8,9]; viscous displacement effects on the inviscid streamlines are not considered. The computed inviscid flow is assumed to be a reasonable approximation to the real mainstream flow so long as turbulent boundary-layer separation does not occur.

Using the standard no-slip and no-mass-transfer boundary conditions, the incompressible axisymmetric boundary-layer equations are solved iteratively using the implicit finite-difference program "E7ET"; transverse curvature effects important for axisymmetric bodies with thick boundary layers are retained but streamwise curvature effects are neglected.[10] A two-layer, implicit eddy viscosity model is used in the turbulent boundary-layer computations.[10]

Boundary-layer transition is predicted by the planar flow Michel-e[9] correlation[7,11] or by laminar separation/assumed turbulent reattachment, whichever occurs first. The assumed turbulent reattachment is based on experimental observation (see Ref. 12, pp. 208, 438, 644). The axisymmetric laminar boundary layer parameters are not Mangler-transformed (see Ref. 12, pp. 235–237) to their equivalent planar flow values since the transformation

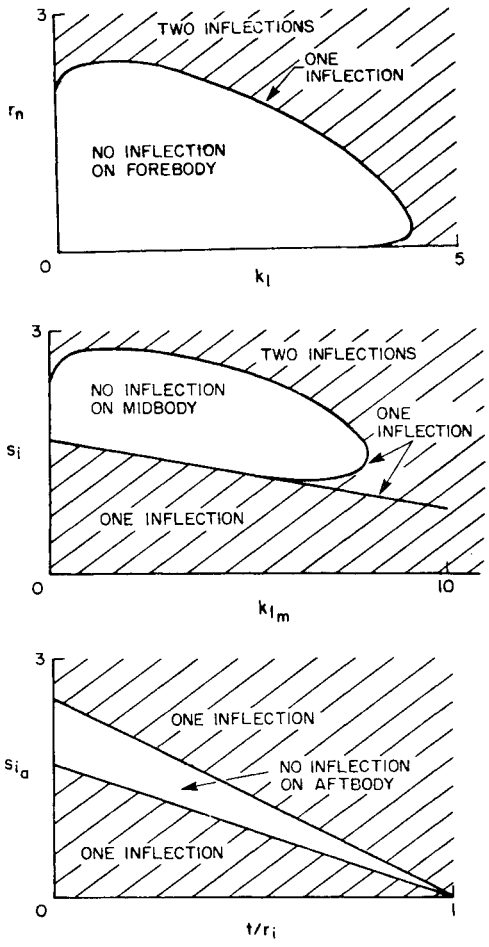


**Fig. 2 Feasible regions for no-inflection constraints on the eight-parameter class of rounded-nose tailboom bodies used in the present study.**

contains an unspecified "arbitrary" constant.

The drag coefficient is computed using Young's formula[13] given as

$$C_D = \frac{\text{Drag}}{1/2\ \rho U_\infty^2 V^{2/3}} = \frac{4\pi}{V^{2/3}} r_o \theta \left(\frac{u_e}{U_\infty}\right)^{(H+5)/2}\Bigg|_{\text{T.E.}} \quad (5)$$

where $C_D$ is the drag coefficient, $\rho$ is the fluid density, $U_\infty$ is the reference velocity, $V$ is the body volume, $r_o$ is the body radius, $\theta$ is the momentum thickness, $u_e$ is the velocity at the edge of the boundary layer, $H = \delta^*/\theta$ is the shape factor, and $\delta^*$ is the displacement thickness. The subscript T.E. denotes quantities at the trailing edge of the body. Since $r_o$, $\theta$, $u_e$, and $H$ vary along the body, the drag coefficient may be treated as $C_D(X)$. Such a treatment is not implied in Young's derivation, but the monotonic behavior of $C_D(X)$ is of interest (see Sec. VI).

The validity of the drag model described here is believed to be limited to nonseparating, tail-boom bodies.

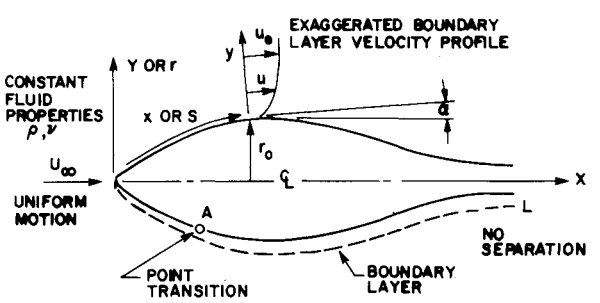


**Fig. 3 Nonseparating flowfield and basic notation considered in the present study.**

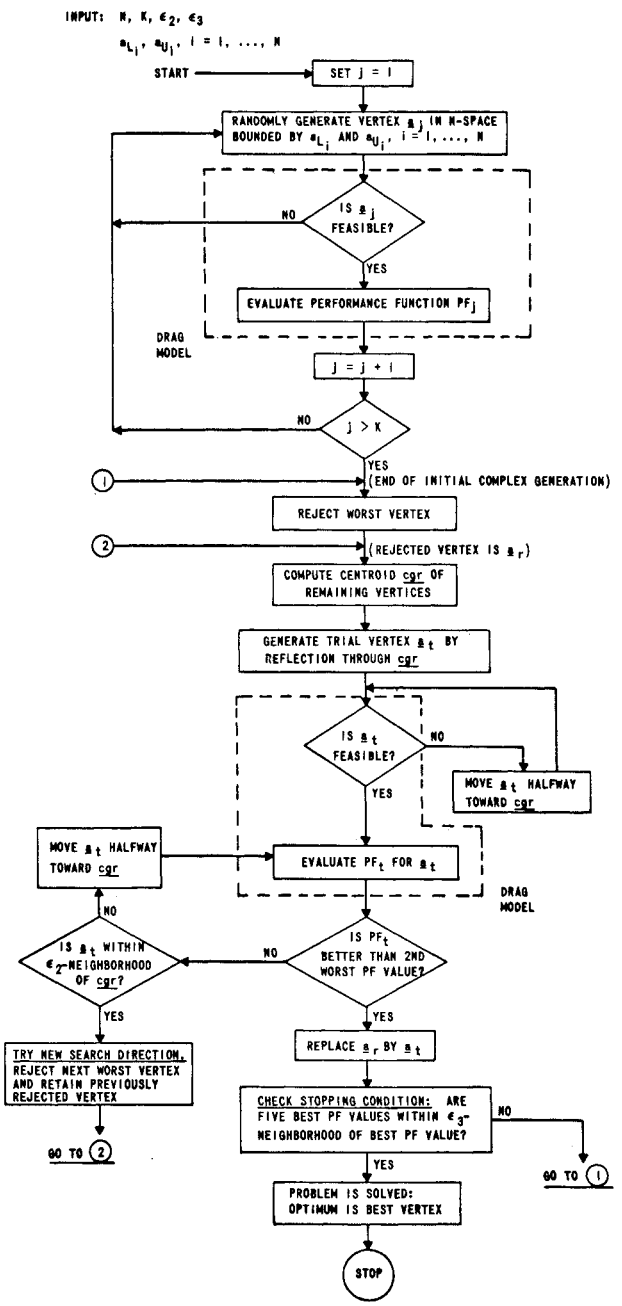


**Fig. 4 Flow chart of the modified Box-Guin Complex Method used in the present study.**

A discussion of the drag model is given in Ref. 7. Experimental drag data are compared with numerical predictions for the Dolphin[3] in Sec. VI.

## V. Optimization Strategy—A Modification of Box's Complex Method

From the optimization point of view, the design problem is

$$\left.\begin{aligned} &\text{Minimize} \quad PF = C_D(a_1,\ldots,a_N) \\ &\text{Subject to} \quad g_l(a_1,\ldots,a_N) \leq 0 \\ &\qquad l = 1,\ldots,NG \gtreqless N \end{aligned}\right\} \tag{6}$$

where the performance function $PF$ is the nonlinear nonanalytic drag coefficient $C_D$, the $a_i$, $i = 1,\ldots,N$, are the independent parameters to be varied, and $g_l$, $l = 1,\ldots,NG$, are the nonlinear, inequality constraints which may or may not be analytic in the parameters. No analytic gradients $\partial C_D/\partial a_i$, $i = 1,\ldots,N$, are available; hence, a nongradient (direct) search method is used since it is believed that nongradient methods are more efficient with "nongradient problems" than finite-differencing used with gradient methods.[14]

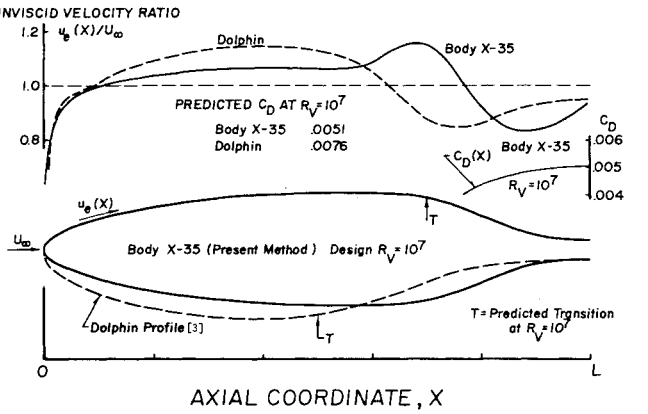


**Fig. 5 Comparison of profiles and velocity distributions for the low-drag laminar body X-35 and the Dolphin.**

For this project we have employed a constrained direct search method rather than one of the unconstrained methods[15-18] used with a penalty function.[14,19] An early method for inequality constrained problems is due to Rosenbrock.[20] In this study, the straightforward Box-Guin Complex Method[21,22] with a modified starting procedure is used. Powell's Method[16] with a penalty function has been used as well as the search strategy described here.

Shown in Fig. 4 is a flow chart of the search strategy. No initial guess is needed. The procedure starts by randomly generating $K$ vertices (body shapes) in the constrained $N$-dimensional space. That is, vertex $j$ has $N$ randomly generated components

$$(a_i)_j = (rn)[a_{U_i} - a_{L_i}] \tag{7}$$

where $i = 1,\ldots,N$, $j = 1,\ldots,K$, $(rn)$ is a random number on the interval [0,1], and $a(L_i)$ and $a(U_i)$ are, respectively, temporary lower and upper parameter boundaries. The vertices are uniformly distributed over the $N$-dimensional rectangular volume defined by the boundaries $a(L_i)$ and $a(U_i)$, $i = 1,\ldots,N$. Normally a portion of the rectangular volume is outside the feasible region defined by the explicit and implicit constraints (geometric and hydrodynamic); when a randomly generated vertex falls outside the feasible region, it is simply thrown out and regenerated. This starting procedure is a modification of Box's Complex Method which calls for an unfeasible vertex to be retracted halfway to the centroid of the partially completed complex figure. The modification was necessary to obtain a well dispersed initial set of $K$ vertices in a nonrectangular feasible search space.

Once the initial complex is formed, the search proceeds by generating the trial vertex $\mathbf{a}_t$ by

$$\mathbf{a}_t = \mathbf{cgr} + \alpha(\mathbf{cgr} - \mathbf{a}_r) \tag{8}$$

where $N$-component $\mathbf{a}_t$ is the new trial vertex, **cgr** is the geometric centroid of the complex figure without the rejected vertex $\mathbf{a}_r$, and the scalar $\alpha$ is the expansion factor. We have used $\alpha = 1.3$ as recommended by Box on empirical grounds.[21] The remaining strategy is summarized in Fig. 4.

Several features of the modified Complex Method make it especially suited to the drag minimization problem. The primary feature is that the method can cope with rather general inequality constraints which are analytic or nonanalytic in the parameters. The method can be programed independently of design constraints and the performance model. The modified starting procedure allows

**Table 1 Geometry and flow data for body $X$-35 at $R_V = 10^7$**

$f_r = 4.848805$ $r_i = 0.647298$
$x_m = 0.588774$ $s_i = 2.286662$
$k_1 = 0.171086$ $x_i = 0.785317$ $L/V^{1/3} = 3.714341$
$r_n = 0.757355$ $t = 0.173127$ Wetted surface area$/V^{2/3} = 6.451445$

| $X/L$ | $Y/L$ | $u_e/U_\infty$ | $\theta/L \times 10^3$ | $H$ | $C_f \times 10^4$ | $R_S \times 10^{-7}$ | $R_\theta \times 10^{-4}$ |
|---|---|---|---|---|---|---|---|
| 0.00019 | 0.00155 | 0.11555 | 0.00788 | 2.21453 | 0.00441 | 0.00066 | 0.00338 |
| 0.00088 | 0.00467 | 0.32147 | 0.00548 | 2.27812 | 0.04880 | 0.00564 | 0.00654 |
| 0.00223 | 0.00772 | 0.48467 | 0.00602 | 2.35099 | 0.10304 | 0.01454 | 0.01084 |
| 0.00418 | 0.01066 | 0.60807 | 0.00681 | 2.38234 | 0.15268 | 0.02623 | 0.01538 |
| 0.00661 | 0.01347 | 0.69484 | 0.00766 | 2.39093 | 0.19184 | 0.03960 | 0.01977 |
| 0.01269 | 0.01878 | 0.80188 | 0.00944 | 2.41548 | 0.23872 | 0.06977 | 0.02812 |
| 0.02890 | 0.02863 | 0.90073 | 0.01320 | 2.47061 | 0.27173 | 0.14195 | 0.04415 |
| 0.05038 | 0.03818 | 0.94806 | 0.01696 | 2.49704 | 0.28698 | 0.23224 | 0.05971 |
| 0.06329 | 0.04301 | 0.96456 | 0.01882 | 2.50424 | 0.29350 | 0.28566 | 0.06744 |
| 0.09414 | 0.05290 | 0.99092 | 0.02261 | 2.51270 | 0.30546 | 0.41272 | 0.08321 |
| 0.11243 | 0.05798 | 1.00211 | 0.02456 | 2.51523 | 0.31069 | 0.48804 | 0.09142 |
| 0.13291 | 0.06315 | 1.01241 | 0.02657 | 2.51723 | 0.31512 | 0.57248 | 0.09993 |
| 0.15551 | 0.06830 | 1.02193 | 0.02864 | 2.51840 | 0.31880 | 0.66585 | 0.10872 |
| 0.17851 | 0.07304 | 1.03008 | 0.03063 | 2.52023 | 0.32038 | 0.76101 | 0.11721 |
| 0.20159 | 0.07733 | 1.03696 | 0.03256 | 2.52255 | 0.32019 | 0.85655 | 0.12541 |
| 0.23636 | 0.08300 | 1.04531 | 0.03538 | 2.52704 | 0.31672 | 1.00021 | 0.13737 |
| 0.27125 | 0.08782 | 1.05162 | 0.03818 | 2.53299 | 0.30972 | 1.14385 | 0.14913 |
| 0.30625 | 0.09186 | 1.05616 | 0.04100 | 2.54058 | 0.29959 | 1.28699 | 0.16084 |
| 0.34132 | 0.09516 | 1.05916 | 0.04389 | 2.54986 | 0.28683 | 1.42922 | 0.17265 |
| 0.37645 | 0.09780 | 1.06082 | 0.04686 | 2.56046 | 0.27222 | 1.57026 | 0.18464 |
| 0.41161 | 0.09981 | 1.06139 | 0.04993 | 2.57160 | 0.25671 | 1.70999 | 0.19686 |
| 0.44681 | 0.10127 | 1.06125 | 0.05308 | 2.58119 | 0.24183 | 1.84861 | 0.20925 |
| 0.48202 | 0.10224 | 1.06094 | 0.05624 | 2.58484 | 0.22994 | 1.98690 | 0.22164 |
| 0.51724 | 0.10280 | 1.06145 | 0.05924 | 2.57325 | 0.22538 | 2.12674 | 0.23357 |
| 0.55247 | 0.10306 | 1.06480 | 0.06167 | 2.52722 | 0.23772 | 2.27277 | 0.24391 |
| 0.58770 | 0.10312 | 1.07692 | 0.06234 | 2.39861 | 0.30109 | 2.43953 | 0.24935 |
| 0.62292 | 0.10291 | 1.11066 | 0.05971 | 2.23787 | 0.40482 | 2.66131 | 0.24631 |
| 0.64639 | 0.10210 | 1.13660 | 0.05830 | 2.20649 | 0.41915 | 2.82260 | 0.24613 |
| 0.66979 | 0.10023 | 1.15388 | 0.05927 | 2.25221 | 0.35837 | 2.96616 | 0.25404 |
| 0.69303 | 0.09687 | 1.15319 | 0.06456 | 2.44806 | 0.20100 | 3.06499 | 0.27651 |
| | | | Transition | | | | |
| 0.70454 | 0.09456 | 1.14417 | 0.08787 | 1.57330 | 2.44932 | 3.09092 | 0.37344 |
| 0.71595 | 0.09182 | 1.12914 | 0.10862 | 1.40741 | 3.27678 | 3.09955 | 0.45554 |
| 0.72726 | 0.08866 | 1.10849 | 0.13570 | 1.37573 | 3.08453 | 3.09121 | 0.55870 |
| 0.74953 | 0.08120 | 1.05395 | 0.21097 | 1.37556 | 2.29089 | 3.03105 | 0.82590 |
| 0.78222 | 0.06806 | 0.96007 | 0.39712 | 1.39904 | 1.32631 | 2.88669 | 1.41616 |
| 0.81472 | 0.05445 | 0.89152 | 0.68201 | 1.41481 | 0.82219 | 2.79723 | 2.25843 |
| 0.84759 | 0.04177 | 0.84925 | 1.08602 | 1.41629 | 0.56509 | 2.77572 | 3.42575 |
| 0.88115 | 0.03108 | 0.83255 | 1.59128 | 1.39303 | 0.43063 | 2.83006 | 4.92082 |
| 0.91550 | 0.02337 | 0.84268 | 2.06113 | 1.34564 | 0.34669 | 2.97478 | 6.45138 |
| 0.95045 | 0.01913 | 0.87511 | 2.25892 | 1.29339 | 0.30584 | 3.20374 | 7.34251 |
| 0.97391 | 0.01806 | 0.90454 | 2.17824 | 1.26369 | 0.31337 | 3.39038 | 7.31837 |
| 0.99576 | 0.01785 | 0.93457 | 2.01739 | 1.24245 | 0.33866 | 3.58447 | 7.00301 |

the method to start with randomly and globally distributed information (body shapes) so that it has some chance of finding a global optimum in the feasible region, although there is no guarantee that such is found. The complex figure's ability to "roll" along boundaries helps to prevent premature convergence on a boundary. Since the method uses large-scale features of the function surface, it is not sensitive to local irregularities and small errors which might confuse local gradient methods. The primary deficiency in the method described here is that the stopping condition, while precisely defined, has proved economically costly to satisfy; the method lacks quadratic convergence. Usually the search is aborted after a large number, e.g., $3N$ to $4N$, of $C_D$ evaluations do not improve the best value. The best vertex is assumed to be a reasonable approximation to the local optimum. The "looseness" of the stopping procedure is normally acceptable for design problems. Small (five percent) parameter perturbations near the reported best design can be used to reveal sensitivity characteristics and to test whether the design is a local optimum.

The role of design constraints is significant for this problem as well as for engineering design in general. The constraints, when properly used, prevent unrealistic optimal solutions. Optimal solutions are no better than the models used in the optimization; those solutions resting on constraint boundaries are no better than the assumptions behind the constraints. The optimization strategy used here is independent of both model and constraints so that the effect on the minimum drag shapes due to changes in either the model or constraints can be studied.

The optimal design philosophy used in the present study views the optimization strategy and the drag model as independent, interacting "black boxes." For example, the search strategy does not know if the computed drag coefficient $C_D$ is the result of a numerical computation or a wind tunnel experiment. The black-box philosophy is useful for complicated problems which defy straightforward analytic understanding; at the present time the drag problem falls into this category.

## VI. Results and Comparisons

In this section we compare a sample design, dubbed "$X$-35," produced by the present method with the Dolphin, an experimentally verified design with half the drag

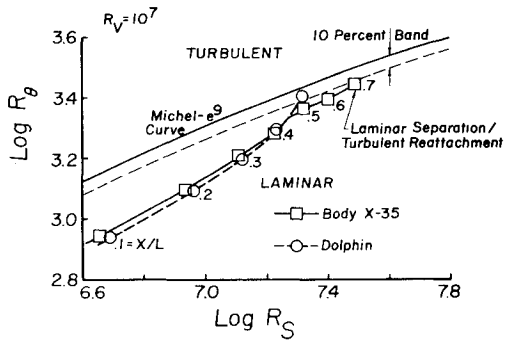


**Fig. 6 Comparison of transition predictions for body $X$-35 and the Dolphin at $R_V = 10^7$ using the Michel-e$^9$ correlation.**

of a conventional torpedo.[3] The results are subdivided into hydrodynamic aspects and optimization aspects.

### Hydrodynamic Aspects

The design $R_V$ of $10^7$ for body $X$-35 corresponds to the Dolphin volume of 5.6 cubic feet at 40 knots in water. Body $X$-35 with its inviscid velocity distribution and $C_D(X)$ are shown in Fig. 5 along with the Dolphin for comparison. The $C_D$ for body $X$-35 is about one-third lower than that of the Dolphin at $R_V = 10^7$. Geometry and flow data at $R_V = 10^7$ for body $X$-35 are given in Table 1. The long run of near-zero velocity gradient suggests that the forebody is similar to a Reichardt section. The region of locally accelerated flow at $X/L = 0.65$, caused by continuous but rapidly changing curvature, suppresses transition until $X/L = 0.7$. The turbulent boundary layer survives the region of decelerated flow without separating and enters the terminal accelerated region in which the velocity $u_e$ asymptotically approaches the freestream value. The $C_D(X)$ computed by Young's formula, Eq. (5), increases monotonically to the trailing edge value of $C_D = 0.0051$.

Transition predictions at $R_V = 10^7$ for body X-35 and the Dolphin are shown in Fig. 6 with the Michel-e$^9$ curve. For body $X$-35, the laminar $R_\theta - R_S$ trajectory never enters the indicated 10% band; transition is predicted by laminar separation and assumed turbulent reattachment. By contrast, the Dolphin laminar $R_\theta - R_S$ trajectory monotonically approaches the curve and crosses it at about $X/L = 0.5$.

Predicted drag coefficients $C_D$ for body $X$-35 and the Dolphin, as well as experimental data for the Dolphin,[3] over a range of Reynolds number $R_V$ are shown in Fig. 7. The reasonably good agreement between predicted and

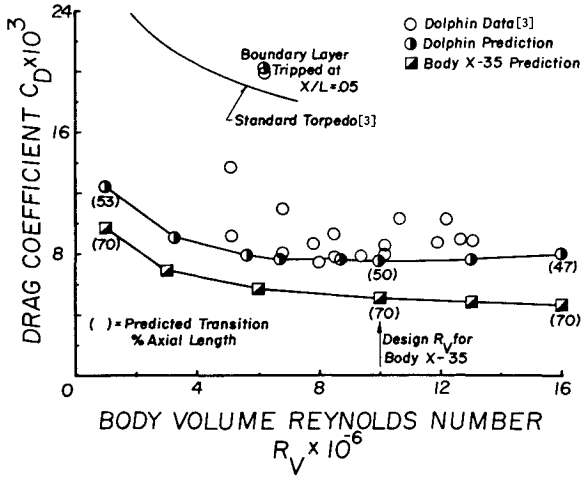


**Fig. 7 Comparison of drag coefficient vs Reynolds number for body $X$-35 and the Dolphin.**

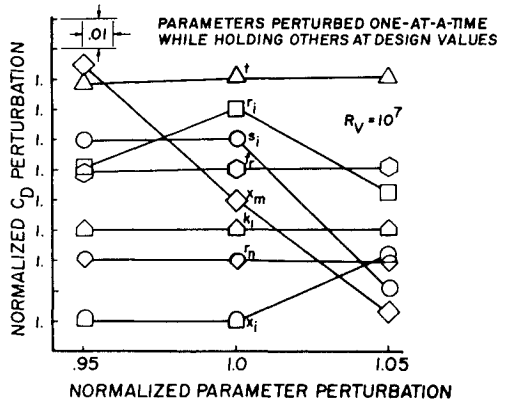


**Fig. 8 Parameter-perturbation studies on the eight-parameter body $X$-35 at its design Reynolds number $R_V = 10^7$.**

experimental values of $C_D$ for the Dolphin indicates validity of the drag model at least over the test $R_V$ range. The experimental and predicted $C_D$ values for the tripped laminar boundary layer are in very good agreement and establish that the Dolphin's low drag is due to extensive laminar flow. The fact that extensive laminar flow can exist in the ocean environment at these high Reynolds numbers is in itself significant. The predicted $C_D$ values for body $X$-35 are one-third lower than those for the Dolphin in this $R_V$ range. The Dolphin's demonstration of laminar flow exploitation combined with the inferred (from Fig. 6) superior laminar stability of body $X$-35 suggests that body $X$-35 is a realistic improvement over the Dolphin body.

### Optimization Aspects

For the sample run given here, the input values were $N = 8$, $K = 16$, $\epsilon_2 = \epsilon_3 = 1\%$, $R_V = 10^7$, and $NN = 30$. The search strategy found body $X$-35 at the 35th $C_D$ evaluation. However, the method was unable to generate a new favorable search direction and the search was terminated without formal convergence after 80 $C_D$ evaluations (80 minutes CPU time on CDC 6500 computer). Such performance suggests that the modified Box-Guin Complex Method is a good starting procedure that may be adequate for design purposes, but that another procedure should be used for formal convergence if it is required.

Perturbation studies on body $X$-35 at its design $R_V = 10^7$ are shown in Fig. 8. A plus and minus five percent perturbation is made on each dimensionless parameter while holding the other seven parameters at their design values given in Table 1. The perturbations reveal that body $X$-35 is suboptimal, a consequence of stopping the search after 80 $C_D$ evaluations without formal convergence. The perturbations also reveal that $C_D$ is locally quite sensitive to the maximum diameter location $x_m$ and the inflection point slope $s_i$. $C_D$ is locally insensitive to the fineness ratio $f_r$, the nose radius $r_n$, the maximum diameter curvature $k_i$, and the dimensionless tail boom diameter $t$. The fact that there is a local maximum in the $r_i$ direction indicates that the $C_D$ surface in the 8-dimensional parameter space is complicated in the neighborhood of body $X$-35.

## VII. Conclusions and Recommendations

A method has been developed for designing minimum drag hull shapes of axisymmetric bodies of revolution. The method incorporates a parametric body description, a drag computation, hydrodynamic constraints, and an optimization scheme in the form of a computer program which produces realistic candidates for low-drag body shapes. The formulation has been designed so that im-

proved drag models, different design constraints, or alternative shape characterizations may be utilized in the design of the minimum drag bodies. Experience with the method has generated the following specific conclusions and recommendations:

1) Low-drag axisymmetric body designs exploiting appreciable runs of laminar flow have resulted from the optimization technique and particular drag model described in this paper.

2) Comparison of the "Dolphin"[3] experimental body data and design and a minimum drag design at the same Reynolds number indicates that the optimization techniques generates realistic candidates for low drag body shapes with significantly less drag (⅓ less drag for a 5.6 $ft^3$ body at 40 knots.)

3) Further work examining body shapes as a function of Reynolds' number indicates that the optimization technique provides an effective low drag body design mechanism for a wide range of parameters.

4) The optimization program has been designed to accept improved drag computations and different design or hydrodynamic constraints.

5) For nonseparating flow on axisymmetric bodies, the drag model used for this work agrees reasonably well with data at moderate Reynolds numbers ($R_V \sim 10^7$).

6) Development of more generally applicable drag models is needed.

7) Development of better drag models and experimental verification of the low-drag designs should be jointly undertaken. Particular attention should be given to the transition criterion from laminar to turbulent flow and the stability of any given long, laminar run.

8) Further work on the optimization scheme could result in more efficient convergence.

## References


[1]Granville, P. S., "Progress in Frictional Drag Reduction, Summer 1968 to Summer 1969," Hydromechanics Lab. TN-143, August 1969, Naval Ship Research and Development Center, Washington, D.C.

[2]Goldschmied, F. R., "Integrated Hull Design, Boundary-Layer Control, and Propulsion of Submerged Bodies," *Journal of Hydronautics,* Vol. 1, No. 1, July 1967, pp. 2-11.

[3]Carmichael, B. H., "Underwater Vehicle Drag Reduction Through Choice of Shape," AIAA Paper 66-657, June 1966.

[4]Gertler, M., "Resistance Experiments on a Systematic Series of Streamlined Bodies of Revolution—For Application to the Design of High-Speed Submarines," DTMB Rept. C-297, April 1950, Naval Ship Research and Development Center, Washington, D.C.

[5]Granville, P. S., "Geometrical Characteristics of Streamlined Shapes," NSRDC Rept. 2962, March 1969, Naval Ship Research and Development Center, Washington, D.C.

[6]Parsons, J. S., "The Optimum Shaping of Axisymmetric Bodies for Minimum Drag in Incompressible Flow," Ph.D. thesis, June 1972, School of Mechanical Engineering, Purdue Univ., Lafayette, Ind.

[7]Cebeci, T. and Mosinskis, G. J., "Calculation of Viscous Drag and Turbulent Boundary-Layer Separation of Two-Dimensional and Axisymmetric Bodies in Incompressible Flows," Rept. MDC-J0973-01, Nov. 1970, Douglas Aircraft Co., Long Beach, Calif.

[8]Smith, A. M. O. and Pierce, J., "Exact Solution of the Neumann Problem. Calculation of Non-Circulatory Plane and Axially Symmetric Flows about or within Arbitrary Boundaries," Rept. ES26988, April 1958, Douglas Aircraft Co., Long Beach, Calif.

[9]Faulkner, S., Hess, J. L., and Giesing, J. P., "Comparison of Experimental Pressure Distributions with Those Calculated by the Douglas Neuman Program," Rept. LB31831, Dec. 1964, Douglas Aircraft Co., Long Beach, Calif.

[10]Cebeci, T., Smith, A. M. O., and Wang, L. C., "A Finite-Difference Method for Calculating Compressible Laminar and Turbulent Boundary Layers," Rept. DAC-67131, March 1969, Douglas Aircraft Co., Long Beach, Calif.

[11]Smith, A. M. O. and Gamberoni, N., "Transition, Pressure Gradient, and Stability Theory," Rept. ES26388, Aug. 1956, Douglas Aircraft Co., Long Beach, Calif.

[12]Schlichting, H., *Boundary Layer Theory,* 6th ed., McGraw-Hill, New York, 1968.

[13]Young, A. D., "The Calculation of the Total and Skin Friction Drags of Bodies of Revolution at Zero Incidence," R. and M. No. 1874, April 1939, Aeronautical Research Council, London, England.

[14]Beveridge, G. S. G. and Schechter, R. S., *Optimization: Theory and Practice,* McGraw-Hill, New York, 1970, Chap. 8.

[15]Hooke, R. and Jeeves, T. A., "Direct Search Solutions of Numerical and Statistical Problems," *Journal of the Association for Computing Machinery,* Vol. 8, No. 2, April 1961, pp. 212-229.

[16]Powell, M. J. D., "An Efficient Method for Finding the Minimum of a Function of Several Variables without Calculating Derivatives," *The Computer Journal,* Vol. 7, No. 2, July 1964, pp. 155-162.

[17]Wozny, M. J. and Heydt, G. T., "A Directed Random Search," ASME Paper 70-WA/Aut-7, 1970. (Also available under the same title as a Ph.D. thesis by G. T. Heydt, Aug. 1970, School of Electrical Engineering, Purdue University, Lafayette, Ind.)

[18]Masters, C. O. and Drucker, H., "Observations on Direct Search Procedures," *IEEE Transactions on Systems, Man, and Cybernetics,* Vol. SMC-1, No. 2, April 1971, pp. 182-184.

[19]Fiacco, A. V. and McCormick, G. P., *Nonlinear Programming: Sequential Unconstrained Minimization Techniques,* Wiley, New York, 1968.

[20]Rosenbrock, H. H., "An Automatic Method for Finding the Greatest or Least Value of a Function," *The Computer Journal,* Vol. 3, No. 3, Oct. 1970, pp. 175-184.

[21]Box, M. J., "A New Method of Constrained Optimization and a Comparison with Other Methods," *The Computer Journal,* Vol. 8, No. 1, April 1965, pp. 42-52.

[22]Guin, J. A., "Modification of the Complex Method of Constrained Optimization," *The Computer Journal,* Vol. 10, No. 4, February 1968, pp. 416-417.